PERFORMANCE OF THE NEW ROLL-IN ROLL-OUT TRANSONIC TEST SECTIONS OF THE NAE 1.5MX1.5M BLOWDOWN WIND TUNNEL.

L.H. Ohman, D. Brown

NATIONAL AERONAUTICAL ESTABLISHMENT
NATIONAL RESEARCH COUNCIL
OTTAWA

ABSTRACT

The transonic test section of the NAE 1.5mx1.5m trisonic blowdown wind tunnel has been completely reconstructed in order to improve the overall performance of the facility in terms of productivity and quality of data acquired. Two test sections have been built in modular form, a 0.38mx1.5m two-dimensional (2D) module and a 1.5mx1.5m three-dimensional (3D) module. These modules are fitted into the original plenum chamber and are easily interchangeable. Both test sections have perforated walls with 60° inclined holes and variable porosity from 6% to 0.5%. Each hole has a splitter plate in the streamwise direction, the purpose of which is to eliminate the strong edgetones that are a typical signature of perforated walls. In contrast, the original test section had fixed porosity of 20.5% and normal holes. Furthermore, the 2D test section had to be assembled inside the 3D test section , that was a permanent fixture in the plenum chamber. This was a very time consuming operation.

Following a brief description of the new Roll-in Roll-out Test Section system, results of calibration of the two test sections are presented and discussed, including Mach number distributions and flow quality data. Wall interference effects, as determined from model forces and boundary pressure measurements, are then analyzed in some detail. Examples of the effect of wall porosity on the interference characteristics are given, including data derived from the original test sections. In the 2D case comparisons are also made with adaptive wall results from the NASA Langley 0.3m cryogenic wind tunnel.

NOMENCLATURE

B	width of 2D test section, Ø.38m
c	reference length, 2D airfoil chord Ø.229m
$C_D = \frac{\text{drag force}}{q*S}$	drag coefficient
$C_L = \frac{\text{lift force}}{q*S}$	lift coefficient
$C_N = \frac{\text{normal force}}{q*S}$	normal force coefficient
$C_p = \frac{P-P_{ref}}{q*S}$	pressure coefficient
M	Mach number
M_{nom}	nominal Mach number
M_{ref}	reference Mach number
$M\infty_T$	test section free stream Mach number
$M\infty_c$	$M\infty_T$ corrected for wall interference
M_{loc}	local Mach number
$\Delta M = M\infty_c - M\infty_T$	Mach number correction due to wall interference
P	local static pressure
P_{ref}	reference static pressure
P_o	stagnation pressure
Por	porosity
$q = 1/2\rho U^2$	free stream dynamic pressure
Re	unit Reynolds number, ft^{-1}
Rec	chord Reynolds number
S	reference area: 2D, Ø.08887m^2/ 3D, Model 1 Ø.1529m^2, Model 2 Ø,1338m^2,
U	free stream mean velocity
u	instantaneous stream velocity
v	sidewall suction velocity
x	streamwise coordinate: origin, 2D, balance centreline, 3D, pitch centre of rotation
y	lateral coordinate: origin, 2D, south sidewall
α	angle of attack
α_g	angle between model chord plane and wind tunnel centreline
α_c	angle of attack corrected for wall interference
α_o	flow angularity, +ve for floor to ceiling flow
$\Delta\alpha = \alpha_c - \alpha_g - \alpha_o$	angle of attack correction due to wall interference
ρ	free stream mean density
σ_M	test section Mach number standard deviation
γ	specific heat ratio, for air =1.4
$\delta M/\delta x$	Mach number gradient
$\delta\alpha/\delta x$	angle of attack gradient
$\bar{}$	above quantity denotes mean value
$\sim$	above quantity denotes fluctuating value

1. INTRODUCTION.

The NAE 1.5mx1.5m trisonic blowdown wind tunnel[1] was conceived in the mid 1950:s[2] and went into full operation in 1963. With the growing interest in transonic aerodynamics a need for testing two-dimensional airfoil models was established and a 2D test section was incorporated in the facility in 1969[3,4]. At that time it was thought that the interest in 2D testing would be sustainable for five, or at the most ten years, so the 2D test section was constructed, for quite a modest cost, as an insert to be assembled inside the 3D transonic test section. However, the 1980:s

Copyright © 1990 by the National Research Council of Canada. Published by the American Institute of Aeronautics and Astronautics, Inc. with permission

arrived without any sign of diminishing interest in testing of 2D airfoils, but rather on the contrary. The assembly and disassembly of the 2D test section was a protracted operation, rendering causing a loss of about 5 weeks test time each year, so it was decided to look for a more effective solution to the process of reconfiguring the transonic test section from 3D to 2D testing and vice versa. A study of a system of easily interchangeable test sections, here coined the Roll-in Roll-out Test Section System, was contracted in 1981 with DSMA International, Toronto. The conclusions were that such a system was indeed viable from both a practical and economic point of view. A full description of the contractual aspects and construction of the system is given in a paper presented at the Canadian Aeronautics and Space Institute's (CASI) Aerodynamics Symposium in December 1989 in Ottawa[5], later issued as a National Research Council (NRC) publication[5].

In the process an important change to the transonic wall configuration was decided upon. After a comprehensive internal study of alternative wall configurations, it was decided to replace the existing perforated walls, having 20.5% porosity with normal holes, with variable porosity walls with slanted holes with splitter plates. The reason for staying with perforated walls rather than slotted walls was to minimize wall interference effects at the Mach number range 1 to 1.4, say, for which no practical wall correction scheme seems to exist.

Up to Mach number one slotted or perforated walls appear to be equally acceptable, but for supersonic Mach numbers the perforated wall is preferable because of its superior shock-wave cancellation characteristics[6]. Also, the NAE experience with the old perforated walls had demonstrated that they were perfectly acceptable for subsonic, sonic and supersonic testing and existing subsonic wall interference correction methods[7,8] could easily be adapted to the new perforated walls.

The purpose of the splitter plates, a narrow streamwise plate that splits the hole in two equal halves, is to eliminate the edgetones that otherwise are a main contributor to noise in a perforated wall test section[9,10].

After a brief description of the Roll-in Roll-out Test Section System, the aerodynamic characteristics of the two test sections are discussed in some detail, in particular static pressure calibration data, flow quality results and wall interference characteristics. Comparisons are made with corresponding data from the original test sections and in the 2D case with data from the NASA Langley 0.3m cryogenic wind tunnel.

2. DESCRIPTION.

Since a full description of the new system is provided in reference 5, only the more salient features will here be discussed. The Roll-in Roll-out Test Section System comprises a 2D test section, a 3D test section, the original transonic plenum chamber, a transporter and a parking area (building annex), Figures 1 to 3. The transfer of a test section from the plenum chamber to the parking area, or vice versa, can be effected in half an hour. However, to actually change the mode of operation from, say, 3D to 2D testing still requires about 2 days due to other considerations. This is still a considerable saving in time compared to the 3 weeks for the original system.

As mentioned in the Introduction, the new test sections have perforated walls with slanted holes with the hole diameter (minor axis of the elliptic holes) = 12.7mm. The hole centreline is inclined 60° from the normal to the wall in the direction of the oncoming flow. The porosity can be varied from 6% to 0.5% by means of sliding throttle plates, Figure 4. The splitter plates are made integral with the holes. The hole pattern is depicted in Figure 5. The narrow strips of "no holes" are where the steel plates are attached to the back-up structure, which also supports the throttle plates.

These types of walls are not unique, very similar walls are used in the Yugoslav T38 1.5mx1.5m wind tunnel[11]. The walls are also equipped with rows of integral pressure orifices for measuring the wall static pressure distribution required for wall interference assessment. Since there was considerable doubt about the usefulness of the data acquired from the integral orifices due to their proximity to the perforations, the walls also have provision for installing static pressure tubes, which have proved to be a satisfactory means for measuring the wall static pressures for the original 20.5% porous walls[7].

The inner walls, made of a low alloy high strength steel, have been given a matt black oxide treatment, that serves as a rust protection and also provides a low reflectivity surface. This latter quality is a requirement for the 3D test section walls when engaging the NAE Optical Tracking System[12], that uses infrared diodes as optical targets in aircraft stores clearance measurements. In this context it should also be mentioned that the 3D test section has provision for a roof mounted sting support, Figure 6.

The 2D test section uses the solid sidewalls from the original 2D test section, but with improved surface finish. Also, the sidewall balances and the wake rake system remains as before, as does the sidewall suction system around the model area[4].

3. FLOW CHARACTERISTICS, 2D TEST SECTION.

3.1 Pressure Distributions

Static pressure measurements were performed over a wide range of conditions:

$$0.12 \leq M \geq 0.9$$
$$1.8\times10^6 \leq Re \geq 35\times10^6$$
$$2\% \leq Por \geq 6\%$$

Pressure distributions were obtained using a centreline mounted static probe, Ø32mm, floor and ceiling mounted static tubes, Ø25mm, and from rows of integral orifices along the floor and ceiling and one of the sidewalls. All probes extended upstream into the contraction part of the test section so that no local blockage was caused by the presence of the probes. The arrangement is fully described in Reference 5. Good agreement was generally observed between the centreline probe and the wall static tube data, while the sidewall data showed a small but consistent deviation in the form of a slightly higher adverse pressure gradient on the upstream part of the wall. The floor and ceiling integral data , however showed very large irregularities to such a degree that they were deemed unusable for determining wall boundary conditions.

Sample data will now be examined in some detail. Figure 7 depicts a typical case of the ceiling static tube data for 6%, 4% and 2%porosity and the corresponding "integral" data for 6% and 2% porosity. The data are presented in the form of Mach number difference between the local Mach number and a reference Mach number determined from a static pressure measured on one sidewall at a station about 5.4 tunnel width upstream of the model location. The static tube data show a small negative gradient that becomes more pronounced downstream of the model location. The downstream gradient increases with increasing porosity. The "integral" data, as mentioned above, show large irregularities, particularly for the 6% porosity case. It should be mentioned that three pressure scans were made for each run condition, demonstrating good repeatability, generally within ±0.001 in ΔM.

The data have been processed to yield the following quantities:

test section Mach number	M_{wT}
test section Mach number gradient	$\delta M/\delta x$
test section Mach number standard deviation	σ_M

using data from one tunnel width upstream to one tunnel width downstream of the balance centreline. These quantities have been listed in Table 1 for a number of wind tunnel runs in order of increasing porosity. No discernable consistent trend with porosity can be seen for the gradient and the standard deviation, except at the highest Mach number, 0.85, where the gradient decreases with increasing porosity,while the standard deviation increases. There is also no consistent trend with Mach number for a given porosity. The last set of data for M=0.7 with Reynolds number varying from 7.5×10^6 to 32×10^6/ft shows no effect of Reynolds number on these quantities. Very similar results were also obtained for the centreline probe data[5].

Generally it can be said that the empty test section Mach number gradient is small and varies between 0.7×10^{-4} and -2×10^{-4} per inch. The standard deviation is of the order 10^{-3}.

A total pressure survey, covering one half width of the test section and a vertical traverse of about two tunnel widths at the wake rake location showed good uniform distribution with deviations from the reference pressure of less than 0.1%.

3.2 Flow Quality

Measurements attributable to test section flow quality included the following:

free stream turbulence (single element hot wire)
free stream static pressure fluctuations (microphone)
sidewall static pressure fluctuations
total pressure fluctuations
sidewall boundary layer characteristics
flow angularity

The flow conditions covered were

$$0.4 \leq M \geq 0.8$$
$$6\times10^6 \leq Re \geq 35\times10^6$$

The frequency response of the instrumentation used for all fluctuating measurements was flat for frequencies up to at least 15kHz. Details of the measuring arrangement and data processing can be found in Ref. 5.

A summary of the results presented in Ref. 5 will here be given. However, the hot wire and microphone data will be discussed in some detail and expanded upon from those given in Ref. 5.Data in the form of mass flux rms, $(\widetilde{\rho u}/\overline{\rho u})_{rms}$, from three single element hot wire probes (Ø=0.0076mm, tungsten), mounted on one sidewall at spanwise stations y/B=0.440, 0.323 and 0.207, as measured from the wall and at the model location area, are listed in tables 2a and 2b. Table 2a shows data for Mach numbers from 0.41 to 0.81 at a fixed Reynolds number, 15×10^6/ft, and 2% porosity, while Table 2b gives data for cases of varying Reynolds number, 6×10^6 to 35×10^6/ft for 2% porosity and varying porosity ,2% to 6%, at a fixed Reynolds number, 15×10^6/ft. The tabulated values are the average values over about ten 2.5 seconds averaging periods. Also indicated in Table 2a is the maximum spread in the mass flux values between individual scans. No consistent trend with Mach number can be discerned, nor is there a convincing case for a trend with Reynolds

number or porosity, Table 2b. In a global sense it can be stated that the mass flux rms value varies between 0.2% and 0.3% and is virtually independent of Mach number, Reynolds number and porosity within the investigated range of these parameters.

The tables also list Cp_{rms} values for the free stream (microphone) and sidewall static pressure fluctuations. As for the mass flux data, no particular trend can be observed. The free stream Cp_{rms} varies between 0.6% and 0.8% and the sidewall Cp_{rms} between 1.4% and 1.6%. This difference is consistent with the fluctuation level to be expected from the turbulent sidewall boundary layer[13].

The microphone and hot wire data have been combined to yield the streamwise velocity fluctuation $\tilde{u}/\bar{u}$, or turbulence intensity, as described in Ref.5, for the Table 2a data, using the mean mass flux value for the three hot wire probes. The data have been plotted in Figure 8, which also gives the expression used for calculating the velocity fluctuations. As most eloquently demonstrated by Jones and Steinback[14], it is important to understand how hot wire data have been processed in order to appreciate the results. They also showed that single wire results can differ considerably from the more reliable three wire probe results. Thus, in the absence of three wire probe results the data in Figure 8 can therefore not be regarded as absolute.

The mass flux and acoustic contributions to the velocity fluctuations are shown separated in Figure 8. It is interesting to see how at low Mach number the mass flux term dominates, while at the higher Mach numbers the acoustic term becomes dominant. At M=0.6 the two terms contribute equally.

In the absence of hot wire data the so called plane wave equation, $(\tilde{u}/\bar{u})_{rms} = (\tilde{p}/\bar{p})_{rms}/\gamma M$ is sometimes used to get an estimate of the velocity fluctuations. Applied to the present data it is found that such a simple estimate gives results very close to the "combined" results for $M \geq 0.6$. Without the hot wire data there would, of course, be no way of knowing how meaningful the "plane wave" estimate would be.

That the splitter plate technique effectively suppresses the edgetones is clearly demonstrated by the power spectral density plots shown in Figure 9. The curve for the "old" test section with normal holes shows a pronounced peak at 6.2 kHz, which is attributed to the edgetones. A second harmonic at 12.5 kHz is also quite pronounced. In the new test section no corresponding peak is present. (The difference in Mach number between the two cases should only have the effect of shifting the peak to a higher frequency). However, a pronounced peak at about 400Hz is seen in the new test section, while there is only a hint of a corresponding peak in the old test section. The origin of this peak can only be speculated upon. It is believed to be in the mixing layer, where the plenum air re-enters the tunnel flow at the diffuser re-entry flaps. In the case of the old test section the plenum pressure is almost identical to the test section static pressure and very little plenum air re-enters. The slanted holes in the new test section forces more air through the plenum chamber and consequently more intense mixing in the re-entry area.

Other flow quality data will now be briefly discussed. The total pressure fluctuations, as measured by a fast response pitot probe located at the model location area, see Table 2a, are compared with the free stream static pressure (microphone) fluctuations in Figure 10 in the form of absolute rms values for Reynolds number 15×10^6/ft. The two values increase in unison with Mach number with the total pressure values being 0.03 to 0.04 psi higher than the static pressure values. The sample spectra in the figure show similar character for the two pressures, with a pronounced peak at about 400Hz. It seems reasonable to surmise that the primary source to the static pressure fluctuations is in the total pressure fluctuations. A plausible origin for the 400 Hz peak was discussed in connection with Figure 9.

A thin sidewall boundary layer is essential for meaningful two-dimensional testing. The data presented in Ref.5 for a typical case, M=0.7, show that with adequate sidewall suction the displacement thickness δ^* at the model location varies from 4mm at low Reynolds number (6×10^6/ft) to 3mm at high Reynolds number(24 to 30×10^6). Without suction δ^* increases to 4.3mm for the high Reynolds number case. The shape factor in all cases is about 1.5. The parameter of importance is, of course, the ratio $2\delta^*/B$, which in this case assumes values of 0.021 to 0.016.

Flow angularity of the free stream[5], as determined from model force measurements with the model in upright and inverted position, show some variation with Mach number and porosity. In any case,it is $\leq 0.17°$ upwash. This is a larger value than for the old facility, $\leq 0.07°$ downwash. No explanation for this difference can be offered.

4. FLOW CHARACTERISTICS, 3D TEST SECTION.

4.1 Pressure Distributions.

As for the 2D test section, static pressure distribution measurements were carried out for a range of conditions,

$$0.2 \leq M \geq 1.3$$
$$3 \times 10^6 \leq Re \geq 13 \times 10^6/ft$$
$$1\% \leq Por \geq 6\%$$

using a centreline mounted probe, wall mounted static tubes near the centreline of each wall and two rows of "integral" orifices. The details of the arrangement is described in Ref.5. Only data below M=1 have been fully analyzed.

As for the 2D case it was found that the empty test section has a small negative Mach number gradient that increases with increasing porosity. A sample case for 2% porosity for a nominal Mach number of 0.9 is shown in Figure 11, in the form of Mach number difference, with the reference Mach number obtained from a pressure measured at an orifice located 1867mm (1.24 tunnel width) upstream of the pitch centre of rotation. Data from two of the static tubes have been omitted in order not to congest the graph. Four repeat scans are overplotted showing good repeatability. The centreline probe data show hardly any gradient over the model location area except for the most downstream part, that is influenced by the model (probe) support. The wall data are somewhat more irregular and higher by about 0.002 to 0.003. The integral data are well comparable to the static tube data and considerably less irregular than those for the 2D case,Figure 7. It appears that for the 3D case the integral wall pressures could be used for wall interference assessment. Why the 2D integral wall pressures are so much more irregular is difficult to explain. The pressure orifices are in both cases at identical locations with respect to the hole pattern. A plausible explanation could possibly be found in the boundary layer thickness, which should be considerably thinner in the 2D case because of the 4 to 1 contraction at the entrance of the 2D test section. However no measurements have as yet been carried out to confirm this situation.

As for the 2D case, a number of wind tunnel runs have been evaluated to yield the test section free stream Mach number, the streamwise Mach number gradient and the standard deviation using the first scan data for the centreline probe over the 1m (40 in) model location area indicated in Figure 11. The results are tabulated in Table 3. The main body of the data is for 2% porosity, the last two cases are for 4% and 6% porosity. There appears to be a trend for the M-gradient to decrease with increasing Mach number and also for it to increase with increasing porosity as shown by the M=0.9 results. No consistent trend with Reynolds number is obvious. The standard deviation is of the order of $1x10^{-3}$ and the M=0.9 results suggest that it increases with increasing porosity. Both the gradient and the standard deviation are of comparable magnitude to corresponding 2D test section values.

4.2 Flow Quality.

Hot wire and static pressure fluctuation (microphone) measurements were performed at Mach numbers from 0.2 to 0.9 for Reynolds numbers $6x10^6$ and $9.5x10^6$/ft and with 6%, 4% and 2% wall porosities. The data have been processed in the same way as for the 2D test section. The microphone data are depicted in Figure 12. For M>0.5 the trend is for the noise level to increase with increasing porosity and increasing Mach number. Data obtained in the original 20.5% porosity test section[10] are also shown for comparison. This curve has a different character with a maximum at M=0.7. At this Mach number there is a 30% reduction in the noise level with the new walls at 2% porosity. The power density spectra in the upper part of the figure show that the major contributions to the noise are in the lower frequency domain, <1kHz, and believed coming from the mixing of the plenum chamber air with the test section air in the diffuser re-entry area. As for the 2D case there is no sign of any edgetones, that would otherwise have shown up as a pronounced peak in the 7 to 9 kHz range.

The mass flux and turbulence intensity data are summarised in Figure 13. The data are presented as vertical bars, since no consistent trend with porosity was found. Both quantities show increasing values with increasing Mach number for M>0.3. As in the 2D case the contribution from the static pressure fluctuations to the turbulence intensity becomes significant at the higher Mach numbers. The turbulence has a minimum of about 0.35% at M=0.3 and increases to about 0.65% at M=0.9. No corresponding data are available for the original test section.

Flow angularity was determined over a rather limited range of flow conditions, $0.6 \leq M \geq 1.0$, $Re=8x10^6$ and 4%, 2% and 1% porosities, from force measurements with a model in upright and inverted position. A small downwash was measured in all cases, with a maximum value of 0.35° at M=0.6 and 4% porosity and a low value of 0.15° at M=1 and 2% porosity. It may be recalled that the 2D test section flow showed an upwash. It is rather puzzling that the flow angularity is of opposite sign in the two test sections, particularly since the geometry upstream of the test sections is identical in both cases.

5. WALL INTERFERENCE CHARACTERISTICS, 2D TEST SECTION.

These were determined using the method of Mokry[7] applied to a series of model force and boundary pressure measurements with a 228.6mm (9in) chord supercritical airfoil model. The characteristics thus determined are corrections to free stream Mach number and angle of attack, ΔM and $\Delta\alpha$ respectively, and corresponding gradients at the 1/4 chord (approx.) location. Data for both 2% and 4% porosities have been analyzed and are compared with corresponding results obtained in the old test section with 20.5% porosity[15].

Figure 14 shows the Mach number and angle of attack corrections for Mach numbers from 0.5 to 0.8 in the form of bar charts. The range of lift coefficient is also given. Both corrections decrease with increasing lift coefficient. The excursions in ΔM are much smaller for the new test section at both 4% and 2% porosity than for the old test section.A certain trend can be seen. For the 2% porosity case at M=0.5 a small negative correction (-0.0025) applies that is virtually independent of the lift coefficient. As the Mach number increases the correction shifts in the positive direction and the excursion increases. The 20.5% and 4% porosity cases show rather similar behaviour apart from the smaller excursions for the 4% porosity case.

The angle of attack corrections are all in the negative direction and the excursions are the smallest for 2% porosity. At the higher Mach numbers there is hardly any difference between the 4% and 20.5% porosity cases.

The Mach number and angle of attack gradients are plotted in a similar fashion in Figure 15. Note that the Mach number gradient behaves non-monotonically with lift while the angle of attack gradient increases monotonically with increasing lift. Also shown in the figure are the limits recommended by Steinle and Stanewsky in AGARD AR-164[16], 0.0006M and 0.03° respectively, based on a required accuracy of 0.0001 in the drag coefficient. The M-gradient criteria is partially met by the 20.5% and 2% walls at M=0.5 and 0.7, while only the 2% porosity wall satisfies the criteria over most of the lift range at the higher Mach numbers. The 4% porosity wall does not measure up to the criteria at any of the Mach numbers. In contrast, it is the 20.5% and 4% porosity walls that most closely meet the 0.03°angle of attack criteria over the investigated lift range, while the 2% porosity wall can only satisfy it at low lift.

The interference characteristics are examined in detail in Figure 16 for the case of M=0.765 and a C_L ~0.7 (close to stall) for the three porosity cases discussed. Also plotted are corresponding results for the same model in the NASA Langley 0.3m cryogenic wind tunnel with 13inx13in adaptive walls[17], Figure 16d. These latter data have been calculated as residual corrections using the procedure developed by Mokry[18]. Note that the scales for fig.d is different from the ones for fig:s a,b and c. The wall pressure distribution is given in all cases as well as representative "empty" tunnel pressure distributions for the perforated wall cases.

Comparing first the ventilated wall cases, it is seen that the ΔM curves are quite different. The largest correction is for the 20.5% porosity , which also shows a positive gradient over the model, while the 4% porosity case shows a negative gradient and the 2% porosity case shows virtually no ΔM correction and no gradient. The $\Delta\alpha$ correction for the 20.5% and 4% cases are almost identical with no appreciable gradient, while the 2% case shows a smaller correction but a noticeable gradient over the model. The case for C_L=0 is also shown in the graphs to provide a reference for judging how the corrections are affected by lift.

The residual corrections for the adaptive wall wind tunnel, fig.d, are quite different in character from those for the perforated walls. The ΔM correction is still negative as for the other cases and of the same magnitude as for the 4% case. However , the gradient is initially negative for the upstream part of the airfoil, then zero at the 1/4 chord point, which is the value listed and then positive over the rear part of the airfoil. Although this gradient is fairly large (|0.009| compared to |0.0022| for the 4% case), it is of the same magnitude but of opposite sign for the forward and rear part of the airfoil and the resultant buoyancy effect is therefore likely negligible. The residual $\Delta\alpha$ correction is small, less than 1/10 in magnitude of those for the ventilated walls. The gradient, however, is significant, 0.175°, and uniform over the chord. This is about twice the value for the 2% case. Although these values may seem large compared to the AGARD[16] recommendation of 0.03°, the resultant estimated change in lift due to the equivalent increase in camber would still be less than 1% for a C_L = 0.7. When judging these results it should be kept in mind that the tunnel height to model chord ratio for the adaptive wall case is 1.44 compared to 6.67 for the ventilated wall cases.

Drag polar data from the various wall configurations are compared in Figure 17 for M=0.765, which is the design Mach number for this airfoil. They show on the whole excellent agreement apart from at the higher C_L values. Unfortunately no drag data are available for the adaptive wall at these higher C_L values. Any difference observed is more likely to be due to small differences, ±0.002, in Mach number than due to differences in wall interference characteristics.

6. WALL INTERFERENCE CHARACTERISTICS, 3D TEST SECTION.

A method similar to the one used for the 2D test section and again developed at NAE[19] has been used for evaluating the wall interference characteristics. In Ref.5 it was applied to series of zero lift cases for a small model with only 0.1% geometric blockage, covering the Mach number range 0.8 to 1.1 (no wall corrections applied for M≥1) and 1% to 6% porosity. The corrected results, reproduced in Figure 18, show good agreement between the various porosity data and also with results obtained in the old 20.5% porosity test section, to which no

corrections were applied. Although not a severe test of wall interference, the results demonstrate that the methods of determining Mach number (from plenum pressure in the old test section and from an upstream reference wall pressure in the new test section) are consistent in both cases.

The case of a larger model at high lift coefficient will now be discussed in some detail. Figure 19 shows the wall pressure distributions and ΔM and $\Delta\alpha$ corrections for four values of porosity, 1% 1.5% ,2% and 4% for M=0.8 and C_L ~1. Two different models were used, Model 1 for the 1%,1.5% and 2% porosity walls and Model 2 for the 4% porosity wall. Both models had 0.5% geometric blockage, but the wing area for Model 2 was 14% less than that for Model 1.

The wall pressures shown on top of each graph were obtained from static pressure tubes mounted near the centreline on the floor, ceiling and each sidewall. The pressures do not "close" downstream so the corresponding boundary values must be obtained by an interpolation procedure that is consistent with the solution of the Laplace equation inside a circle[19], in order to carry out the wall interference calculations. As would be expected, the pressure signature is the strongest for the lowest porosity wall. The ΔM and $\Delta\alpha$ values listed apply to the pitch centre of rotation of the model (the vertical dotted line) and are quite small in all cases. However , as the graphs show, the variations in ΔM and $\Delta\alpha$ over the length of the model can be quite significant. The following table lists the corrections for the four cases at the centre of the model and the corresponding maximum variations over the length of the model.

Por.%	ΔM(ctr)	ΔM(var)	Δα°(ctr)	Δα°(var)
1	-0.0001 (1)	0.0141 (141)	0.096 (96)	0.55 (55)
1.5	-0.0049 (50)	0.0060 (61)	-0.036 (36)	0.34 (34)
2	-0.0046 (47)	0.0038 (39)	-0.161 (166)	0.27 (28)
4	-0.0039 (47)	0.0048 (58)	0.341 (412)	0.71 (89)

The numbers in brackets are the values adjusted to the same C_L (=1) and the same wing area, assuming that the corrections are proportional to C_L and wing area. Overall the 2% porosity case shows the best characteristics with the smallest variations in ΔM and $\Delta\alpha$ over the length of the model. The 1% case that shows virtually zero ΔM(ctr) correction exhibits the largest ΔM(var). From the wall interference point of view it must be considered far more important to minimize the variations in the corrections to M and α over the entire model than to minimize them at the centre of the model.

In the figure are also shown the zero lift curves for ΔM and $\Delta\alpha$. As can be seen, the lift effect on ΔM is fairly small while it is quite pronounced on $\Delta\alpha$. It is also interesting to note that the general character of the ΔM and $\Delta\alpha$ curves are the same in all cases. This is in contrast to the 2D situation where the ΔM curves are quite different for the 2% and 4% cases, Figure 17. Unfortunately, no corresponding data for the old 20.5% porosity walls are available at this Mach number. However, available results for M=0.5 for model 1 include 20.5% as well as 2%, 1.5% and 1% wall porosity and are plotted in Figure 20. At this lower Mach number the porosity value seems to have a minute effect on the ΔM curve. The correction at the model centre varies between -0.002 for 1% and -0.003 for the other porosity values. The variation in ΔM is less than 0.002 in all cases. The $\Delta\alpha$ correction, however shows large dependency on the porosity value. The correction at the model centre varies from 0.28° for 1% to -0.20° for 20.5% porosity and the variation over the length of the model is the largest, 0.71°, for 1% and smallest, 0.17°, for 20.5% porosity.

These two examples show that the 3D wall interference effects at subsonic speed are not overly sensitive to the value of wall porosity and also that the "optimum" porosity may vary with Mach number. For the M=0.5 case it may be speculated that for the slanted hole wall the optimum porosity is likely between 2% and 6% (the upper limit of present walls), but these conditions have not yet been explored.

Of interest is to note the similarities of, as well as the differences between the 2D and 3D cases.Both "empty" test sections have a small negative Mach number gradient (positive pressure gradient) of the same magnitude,that becomes more pronounced at the downstream end. The old test sections with 20.5% porosity and normal holes had virtually no gradient.

With the models installed and under high lift conditions the Mach number gradient along the test sections can be characterized as follows:

2D test section, 1.8% geometric blockage, M=0.8

	Mach number gradient		
porosity %	upstream	at model	downstream
2	neg.	0	neg.
4	neg.	neg.	neg.
20.5	neg.	pos.	pos.

3D test section, 0.5% geometric blockage, M=0.8

	Mach number gradient		
porosity %	upstream	at model	downstream
1	0	pos.	pos.
1.5	0	pos.	pos.
2	neg.	0	0
4	neg.	0	pos.

3D test section, 0.5% geometric blockage, M=0.5

	Mach number gradient		
porosity %	upstream	at model	downstream
1	0	0	0
1.5	0	0	pos.
2	0	0	pos.
20.5	0	0	pos.

Upstream the gradient is always negative or close to zero in both test sections. At the model it varies with porosity, in the 2D case from zero at 2% to

negative at 4% and positive at 20.5% porosity. For the 3D test section the gradient is zero except for the two lower porosities at M=0.8. downstream the gradient in the 2D case is negative for 2% and 4% but positive for 20.5% porosity, while in the 3D case it is always positive.

The most surprising feature in the above picture is the downstream gradient that is negative in the 2D case for 2% and 4% porosity in spite of the large geometric and what must also be large wake blockage, while it is always positive in the 3D case with a much smaller blockage. For the 20.5% cases this gradient is always positive. In the latter case the positive gradient can be related to, in addition to the model wake blockage effect, the inflow of plenum air into the test section through the normal hole perforated walls, that provide virtually no resistance to inflow. This inflow,which has no initial momentum in the streamwise direction, causes additional blockage. In the new test sections with slanted holes a corresponding inflow can only take place providing the plenum pressure exceeds the test section pressure by a significant amount. The pressure difference between the plenum pressure and test section pressure was found to be larger in the 3D case than in the 2D case, so there is more likelihood for inflow with the slanted hole walls for the 3D test section.

7. CONCLUSIONS.

The incorporation of the Roll-in Roll-out Test Section System represents a major enhancement of the transonic testing capabilities of the NAE 1.5mx1.5m trisonic wind tunnel. The final design and the construction phases of this project were largely completed within cost and projected time frame. The system has been in operation since May 1989. It comprises a 2D and a 3D test section, a transporter, the original plenum chamber and a parking area. Both test sections have perforated walls with slanted holes with integral splitter plates. The porosity can be varied between 6% and 0.5%.

The two test sections have been calibrated with respect to "empty tunnel" pressure distributions and flow quality and also with respect to wall interference characteristics. Only data for M<1 have so far been analyzed.

Both test sections have good uniform pressure distributions with a small negative streamwise Mach number gradient (positive pressure gradient) of the order of 10^{-4}/in ($4x10^{-3}$/m) over the model test area. The integral pressure data show such large irregularities for the 2D test section that they are deemed unusable for wall interference assessment. However, the corresponding 3D data appears to be acceptable, but no attempt has as yet been done to use them in wall interference calculations.

Hot wire measurements show that the mass flux rms varies between 0.2% and 0.3% in the 2D case and between 0.3% and 0.45% in the 3D case, with the values increasing with Mach number.The acoustic (microphone) data show that the splitter plates effectively eliminate the edgetones, but they also show increased contributions in the lower frequency domain compared to the old test section. This lower frequency contributions are believed generated in the diffuser re-entry area by the mixing of plenum air with test section air. This mixing is more intense for the slanted hole walls, which force more air through the plenum than do the normal hole walls.

The acoustic noise level in the 3D test section generally increases with increasing porosity. At M=0.7 and 2% porosity it is about 30% less than for the old test section, but this favourable difference is more or less negated for M≥0.8. No corresponding comparison can be made for the 2D test section due to incompleteness of data.

The wall interference studies showed that, overall, the 2% porosity walls have the most favourable interference characteristics for both the 2D and 3D test sections.

On the whole, the new test section system has lived up to its expectations and functioned most satisfactorily during its first year of operation. It has untapped potential yet to be explored, such as the possibility of using unequal porosity for floor and ceiling in the 2D test section, as discussed by Mokry[21]. As shown by Williams and Parkinson[22], a solid floor and a suitably ventilated ceiling can produce near interference free data for high lift airfoil models at low speed.

ACKNOWLEDGEMENT

The authors are indebted to the staff of the High Speed Aerodynamics Laboratory of the NAE, in paricular to Y. Y. Chan, F. A. Ellis, R. D. Galway, S. Hashim, M. Khalid, A. Malek, M. Mokry, N. Tang and J. Thain, for their contributions in obtaining the material presented in this document.

REFERENCES

1. Brown, D. — Information for Users of the National Research Council's 5Ftx5Ft Blowdown Wind Tunnel at the National Aeronautical Establishment. Third Edition NAE LTR-HA-6, Sept. 1977

2. Lukasiewics, J. — Canada's Encounter with High Speed Aeronautics. The International Quarterly of the Society for the History of Technology, Technology and Culture, April 1986, Vol.27, No 2, The University of Chicago Press

3. Ohman, L. H. — The NAE High Reynolds Number 15inx60in Two-Dimensional Test Facility. NAE LTR-HA-4, April 1970

4. Ohman, L. H. Brown, D. — The NAE High Reynolds Number 15"x60" Two-Dimensional Test Facility; Operating Experiences and some Representative Results. AIAA Paper No 71-293, March 1971

5. Ohman L.H. et al. — New Transonic Test Sections for the NAE 5Ft x 5Ft Trisonic Wind Tunnel. Proceedings of the First Canadian Symposium on Aerodynamics, Paper No 34, CASI, Ottawa, Dec. 1989, also National Research Council, NAE-AN-62, Jan. 1990

6. Goethert, H. B. — Transonic Wind Tunnel Testing. AGARDograph No 49, Pergamon Press, 1961

7. Mokry, M. Ohman, L.H. — Application of the Fast Fourier Transform to Two-Dimensional Wind Tunnel Wall Interference. AIAA J. of A. Vol.17, No 6, June 1980

8. Mokry, M. — Subsonic Wall Interference Corrections for Finite Length Test Sections Using Boundary Pressure Measurements. AGARD-CP-335, Paper No 10, Sept. 1982

9. Dougherty, Jr. N.S. Anderson, C. F. Parker, Jr. R.L. — An Experimental Study on Suppression of Edgetones from Perforated Wind Tunnel Walls. AIAA Paper 76-50, Jan. 1976

10. Ohman, L. H. Brown, D. Bowker, A. Ellis, F. A. — Recent Improvements to the NAE 5Ftx5Ft Blowdown Wind Tunnel. National Research Council, NAE-AN-31, Aug. 1984

11. Medved, B. Elfstrom, G. M. — The Jugoslav 1.5m Trisonic Blowdown Wind Tunnel. AIAA Paper 86-0746-CP, Jan. 1986

12. Brown, D. Bureau, J. L. — The NAE System for Grid Measurements of External Store's Forces. AIAA Paper 88-2064, May 1988

13. Willmarth, W. W. — Pressure Fluctuations beneath a Turbulent Boundary Layer. Annual Review of Fluid Mechanics, Vol.7, 1975

14. Jones, G. S. Stainback, P. C. — A New Look at Flow Quality for Transonic Flow. SAE Technical Paper Series 881452, Oct. 1988

15. Chan, Y. Y. — Wind Tunnel Investigation of CAST 10-2/DOA-2 12% supercritical Airfoil Model. National Research Council, NAE LTR-HA-5x5/0162, May 1986

16. Steinle, F. Stanewsky, E. — Wind Tunnel Flow Quality and Data Accuracy Requirements. AGARD-AR-184, ed. by R. Dietz, Nov. 1982

17. Mineck, R. E. — Wall Interference Tests of a CAST 10-2/DOA-2 Airfoil in an Adaptive Wall Test Section. NASA TM 4015, Dec. 1987

18. Mokry, M. — Residual Interference and Wind Tunnel Wall Adaptation. AIAA 89-0147, Jan. 1989

19. Mokry, M. — Subsonic Wall Interference Corrections for Finite-Length Test Sections Using Boundary Pressure Measurements. AGARD-CP-335, Paper No.10, Sept. 1982

20. Chan, Y. Y. Tang, N. — Private Communications, 1987

21. Mokry, M. Chan, Y. Y. Jones, D. J. — Two-Dimensional Wind Tunnel Wall Interference. AGARD-CP-281, Chapter 5, Nov. 1983

22. Williams, C. D. Parkinson, G. V. — Low Correction Wall Configuration for Airfoil Testing. AGARD-CP-174, Paper No 21, Sept. 1975

TABLE 1 CEILING STATIC TUBE PRESSURE CALIBRATION RESULTS, 2D TEST SECTION

M_{nom}	$Re*10^6/ft$	Porosity %	$-1 \leq x/B \geq 1$ (B=0.38m/15in)		
			M_{∞_T}	$\delta M/\delta x*10^4$ /in	$\sigma_M * 10^3$
0.40	15	2	0,393	-0.9	1.10
0.40	15	3	0.398	-1.4	1.53
0.40	15	4	0.394	-0.4	1.23
0.40	15	6	0.394	-0.9	1.54
0.70	24	2	0.688	-1.4	1.72
0.70	24	3	0.699	-2.0	2.37
0.70	24	4	0.689	-1.5	1.91
0.70	24	6	0.691	0.3	2.25
			0.802		
0.80	26	2	0.803	-1.0	1.28
0.80	26	3	0.802	-1.6	2.21
0.80	26	4	-	-1.7	2.08
0.80	26	6		-	-
			0.857		
0.85	27	2	0.857	-1.7	2.02
0.85	27	3	0.841	-1.4	2.10
0.85	27	4	0.840	-1.1	2.19
o.85	27	6		0.7	2.94
			0.700		
0.70	7.5	2	0.688	-1.4	1.62
0.70	24	2	0.700	-1.4	1.72
0.70	32	2		-1.3	1.52

TABLE 2a 2D TEST SECTION FLOW QUALITY RESULTS
2% POROSITY Re = 15 X 10^6/ft

MACH No.	Mass flux			Static pressure			Total pressure
	% $(\widetilde{\rho u}/\overline{\rho u})_{rms}$			Centre-line		Sidewall	
	Probe 2	Probe 3	Probe 4	Cp_{rms} %	$(\widetilde{p}/\overline{p})_{rms}$ %	Cp_{rms} %	$\widetilde{Po}_{rms}$ psi
	$y/_B$=.44	0.323	0.207				
0.41	* +2 0.27 -3	+3 0.22 -2	+4 0.26 -4	+3 0.58 -1	0.068	+7 1.35 -4	+6 0.089 -5
0.51	+1 0.23 -3	—	+3 0.24 -3	+1 0.63 -1	0.115	+1 1.36 -1	+1 0.111 -2
0.61	+2 0.21 -2	+1 0.29 -1	+2 0.17 -1	+2 0.78 -1	0.203	0 1.44 -1	+1 0.135 -1
0.71	+5 0.28 -2	+2 0.29 -2	+2 0.20 -2	+3 0.82 -3	0.289	+1 1.40 -2	+1 0.149 -1
0.81	+5 0.28 -2	+2 0.29 -2	+2 0.20 -2	+3 0.77 -1	0.354	+3 1.32 -2	+4 0.151 -3

* The ± figures indicate the spread in the last digit over about ten 2.5 second averaging periods.

TABLE 2b 2D TEST SECTION FLOW QUALITY RESULTS, M = 0.81

Por. %	Re*10^{-6} /ft	Mass flux fluctuations				Static pressure	
		% $(\widetilde{\rho u}/\overline{\rho u})_{rms}$				centre line	side wall
		Probe 2	Probe 3	Probe 4	Average	% Cp_{rms}	% Cp_{rms}
		y/B=.44	.323	.207			
2	6	Ø.23	Ø.18	Ø.16	Ø.19	-	1.37
2	15	Ø.28	Ø.29	Ø.2Ø	Ø.26	Ø.77	1.35
2	35	Ø.34	Ø.23	Ø.17	Ø.25	-	1.47
2	15	Ø.28	Ø.29	Ø.2Ø	Ø.26	Ø.77	1.32
4	15	Ø.3Ø	Ø.27	Ø.23	Ø.27	-	1.66
6	15	Ø.32	Ø.26	Ø.35	Ø.31	-	1.54

TABLE 3 CENTRE-LINE STATIC PRESSURE CALIBRATION RESULTS
3D TEST SECTION

Run#	M_{nom}	Re x 10^{-6} /ft	Porosity %	$-25" \leq x \leq 15"$		
				$M_{\infty T}$	$\delta M/\delta x * 10^4$ in^{-1}	$\sigma_M * 10^3$
35045	0.50	6.0	2	0.512	-0.82	1.30
35046	0.50	9.5	2	0.512	-1.09	1.48
35047	0.50	13.0	2	0.512	-1.08	1.42
35051	0.70	6.0	2	0.718	-0.38	0.69
35052	0.70	9.5	2	0.719	-0.55	0.98
35053	0.70	13.0	2	0.720	-0.10	0.77
35054	0.80	13.0	2	0.821	-0.68	1.18
35055	0.90	9.5	2	0.923	-0.35	1.12
35056	0.90	13.0	2	0.925	-0.50	1.14
35014	0.97	10.0	2	0.987	-0.14	0.91
35057	0.90	9.0	4	0.928	-0.63	1.49
35066	0.90	9.0	6	0.942	-1.15	1.69

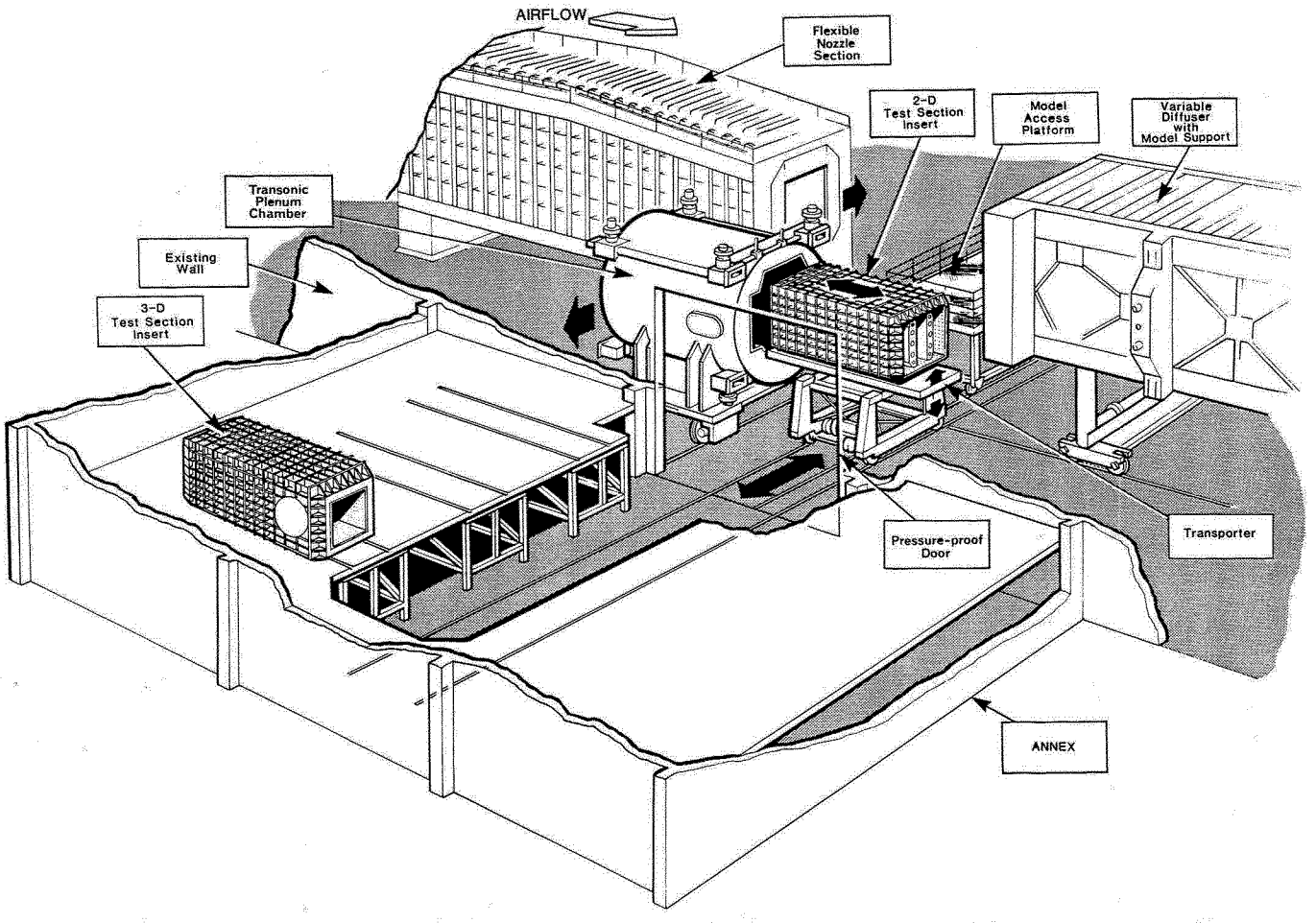

FIG. 1: ROLL-IN ROLL-OUT TEST SECTION SYSTEM, NAE 1.5 m x 1.5 m WIND TUNNEL

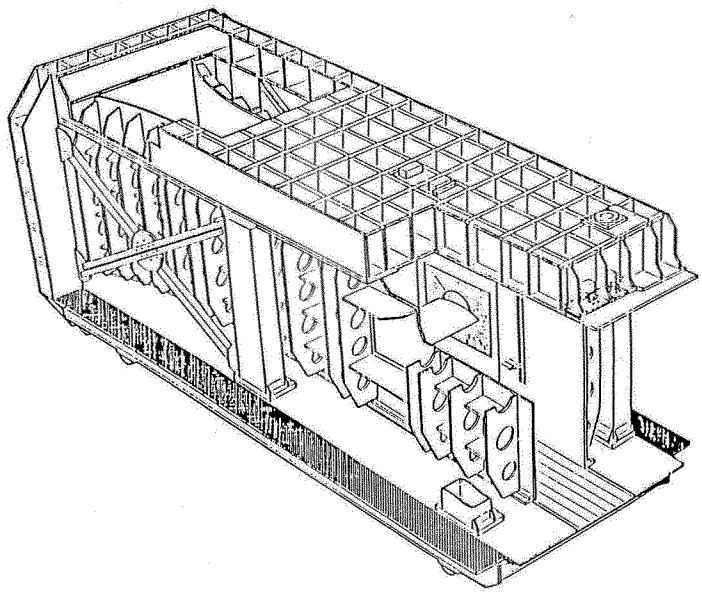

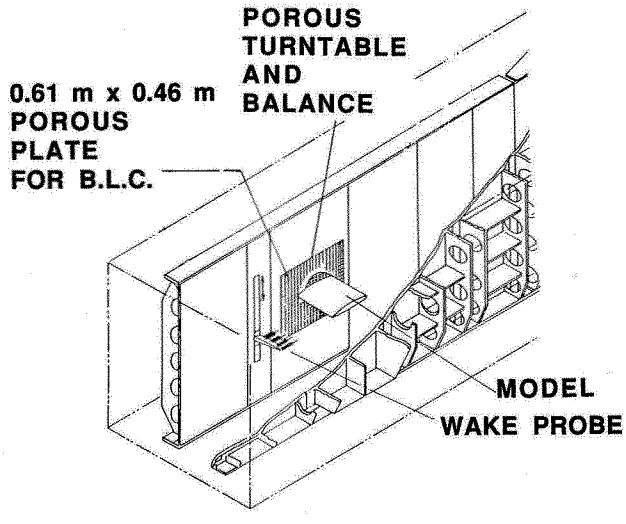

FIG. 2: 0.38 m x 1.5 m 2D TEST SECTION

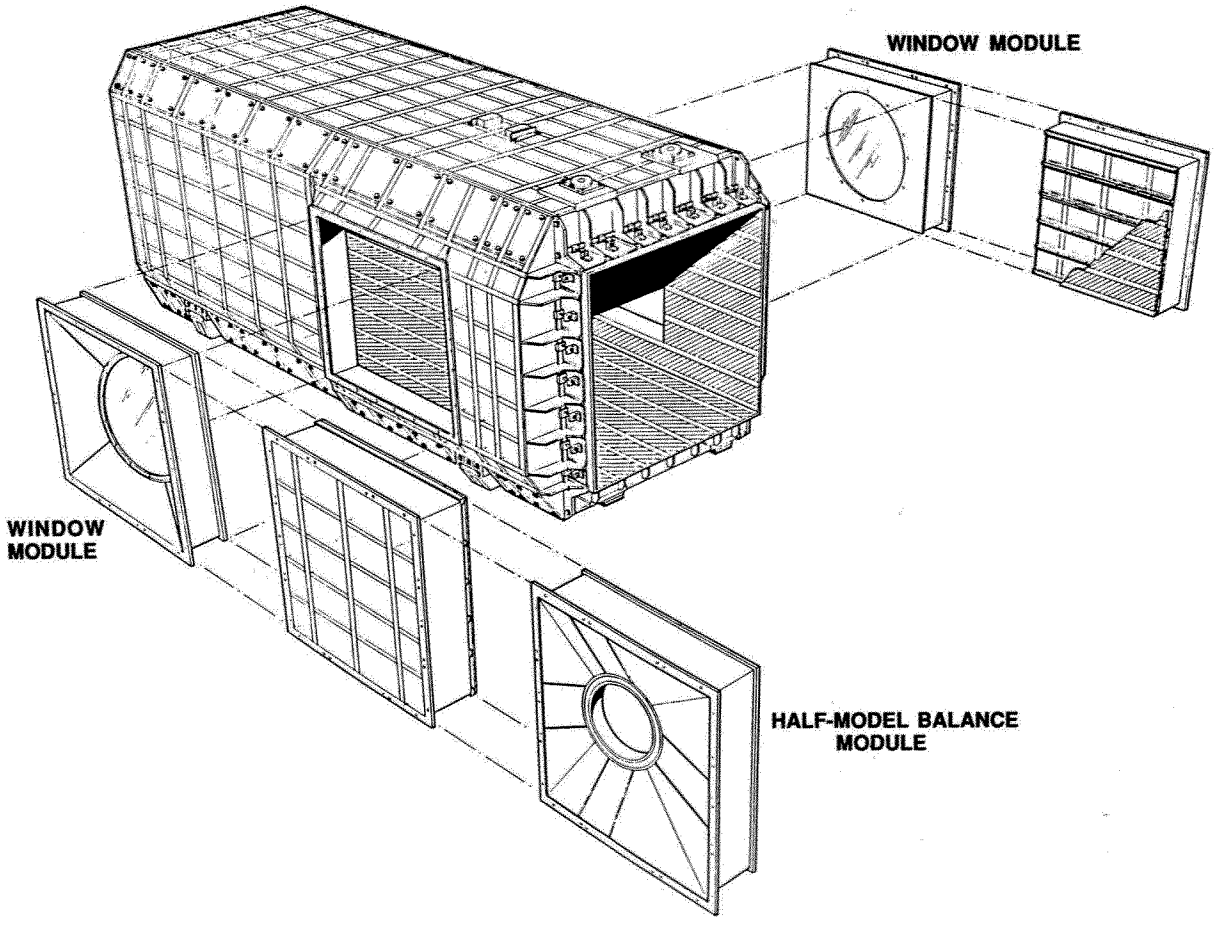

FIG. 3: 1.5 m x 1.5 m TEST SECTION

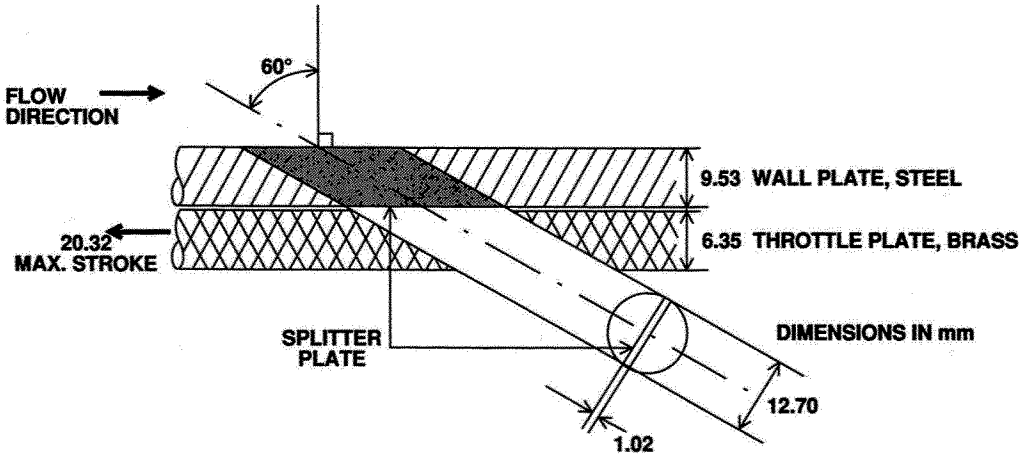

FIG. 4: VARIABLE POROSITY WALL HOLE GEOMETRY

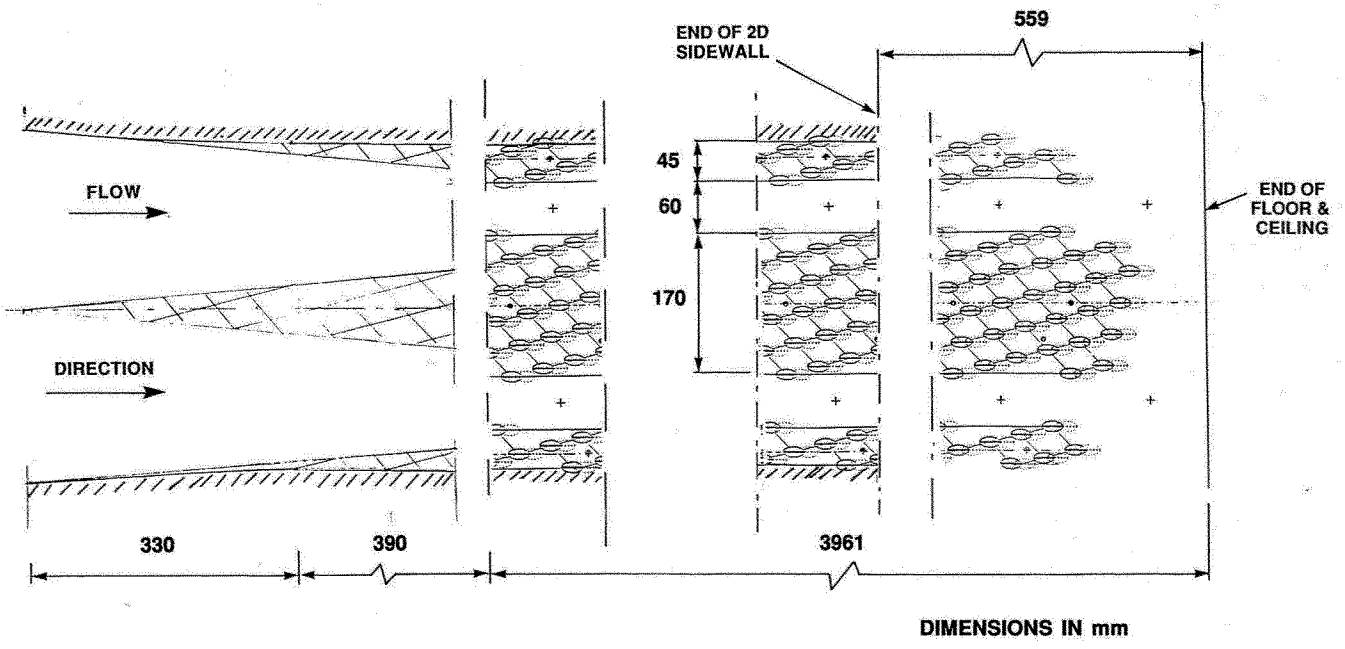

FIG. 5: PERFORATED WALL HOLE PATTERN: 2D INSERT FLOOR AND CEILING (3D WALLS HAVE FIVE 170 mm WIDE PERFORATED STRIPS AND TWO 145 mm WIDE END STRIPS)

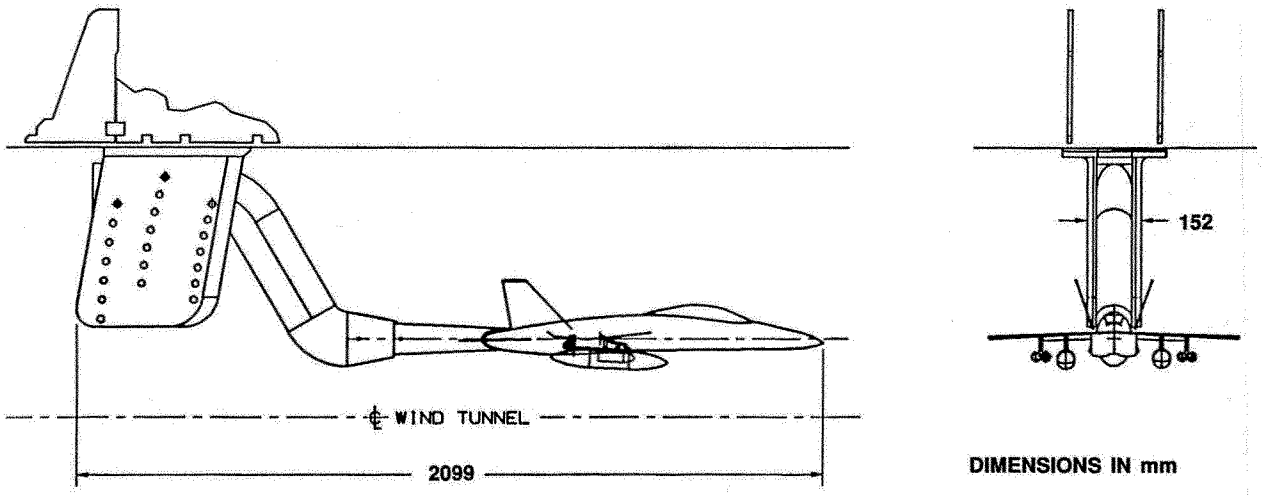

FIG. 6: ROOF MOUNTED STING

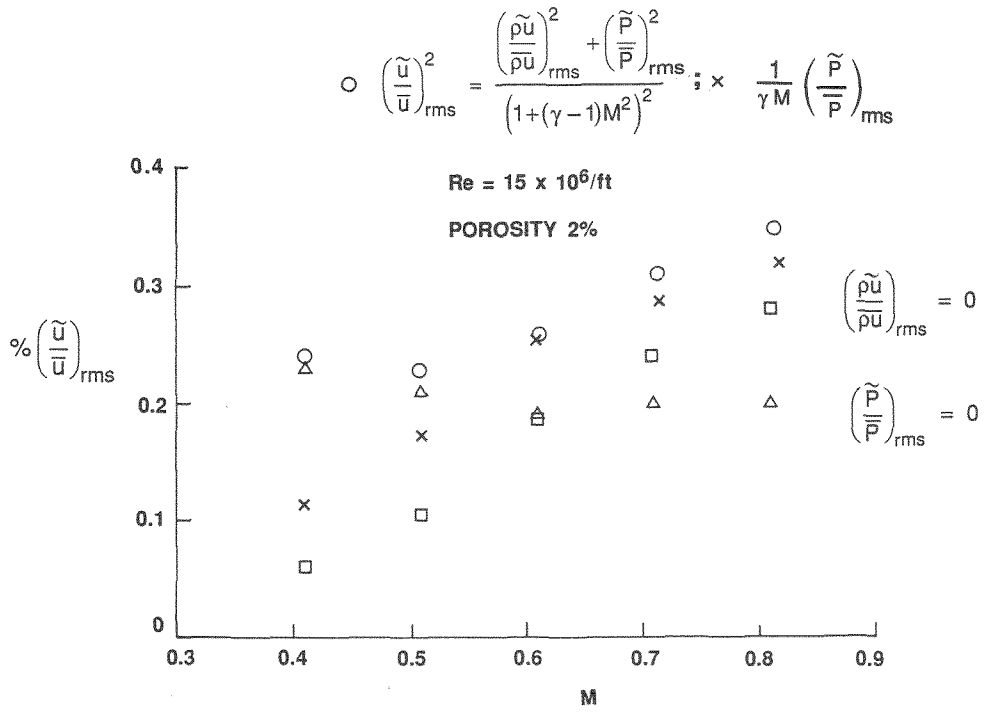

FIG. 8: 2D TEST SECTION TURBULENCE RESULTS

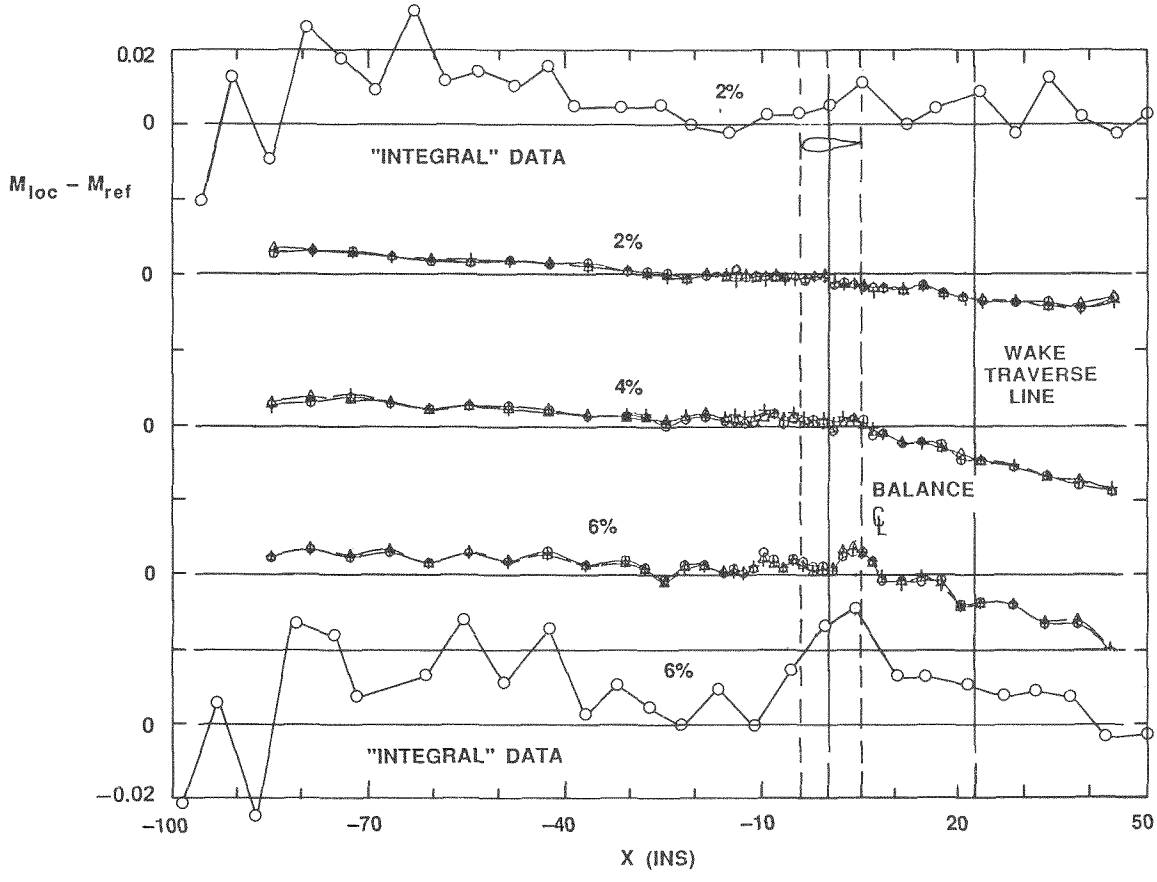

FIG. 7: 2D CEILING MACH NUMBER DISTRIBUTION AT M_{nom} = O.7, Re = 24 x 10^6 ft^{-1}

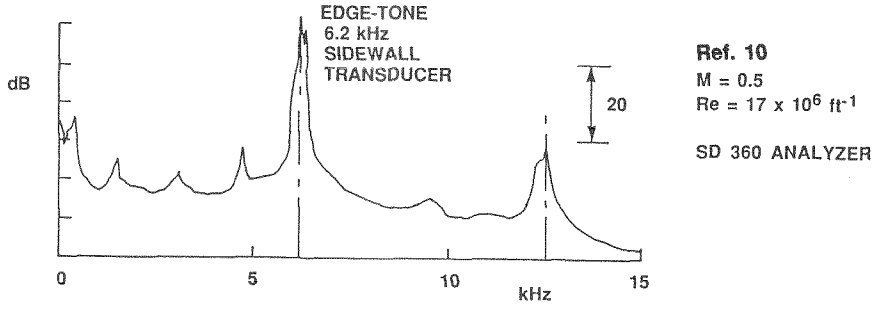

(a) 'OLD' TEST SECTION, 20.5% POROSITY (NORMAL HOLES)

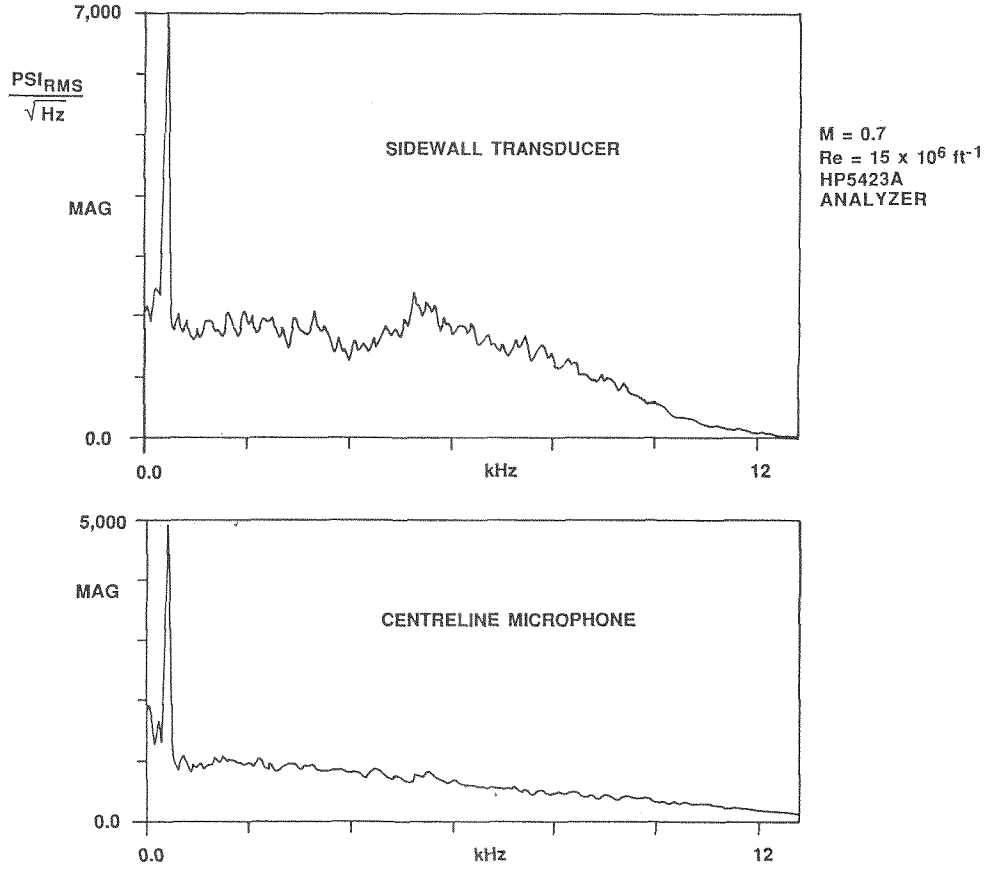

(B) NEW TEST SECTION, 2% POROSITY

FIG. 9: POWER SPECTRAL DENSITIES, 2D TEST SECTION

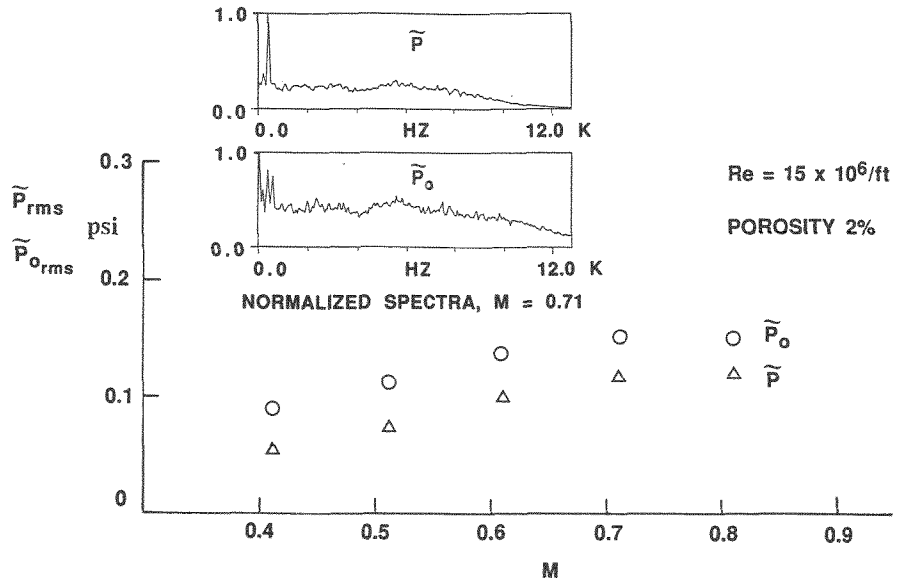

FIG. 10: ABSOLUTE LEVEL OF 2D TEST SECTION STATIC AND TOTAL PRESSURE FLUCTUATIONS

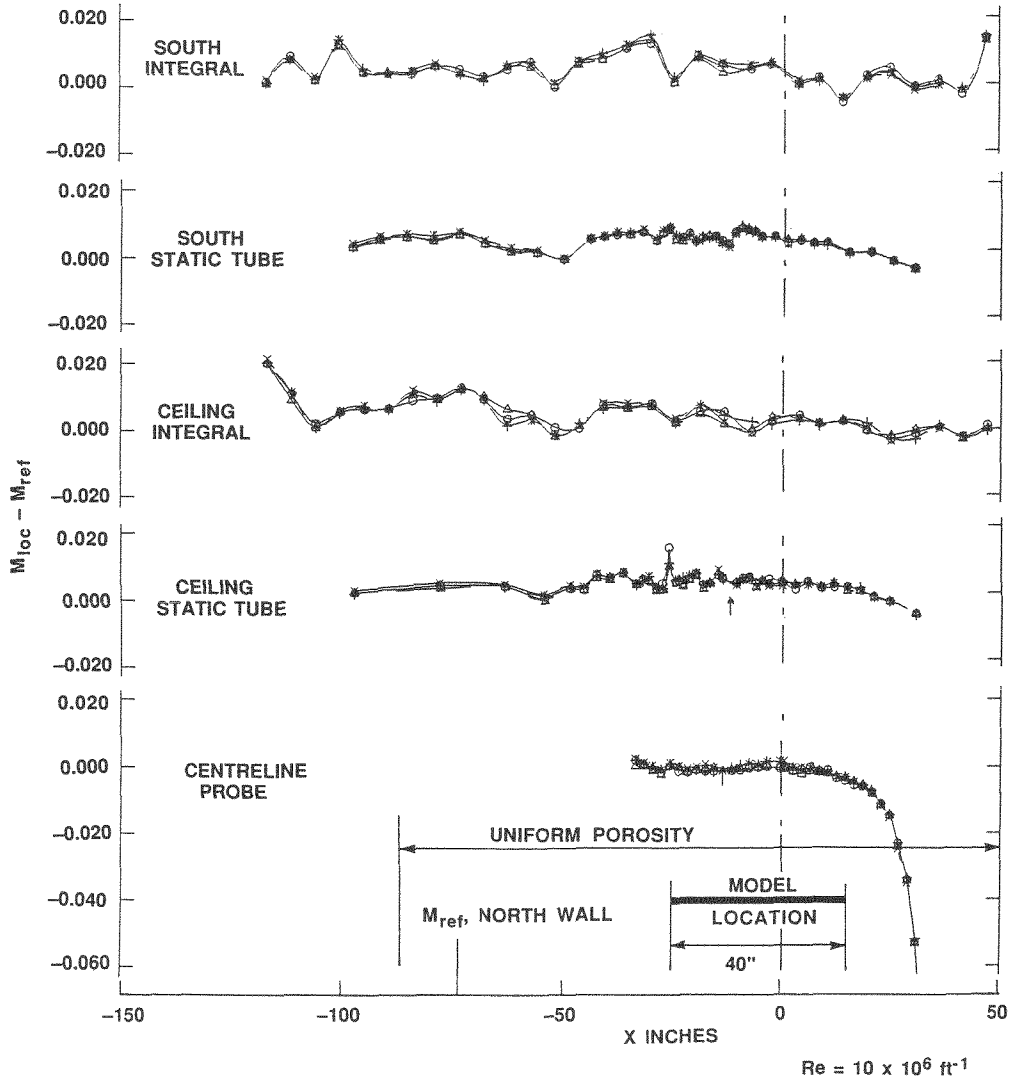

FIG. 11: MACH NUMBER DISTRIBUTION, M_{nom} = 0.9, 3D TEST SECTION

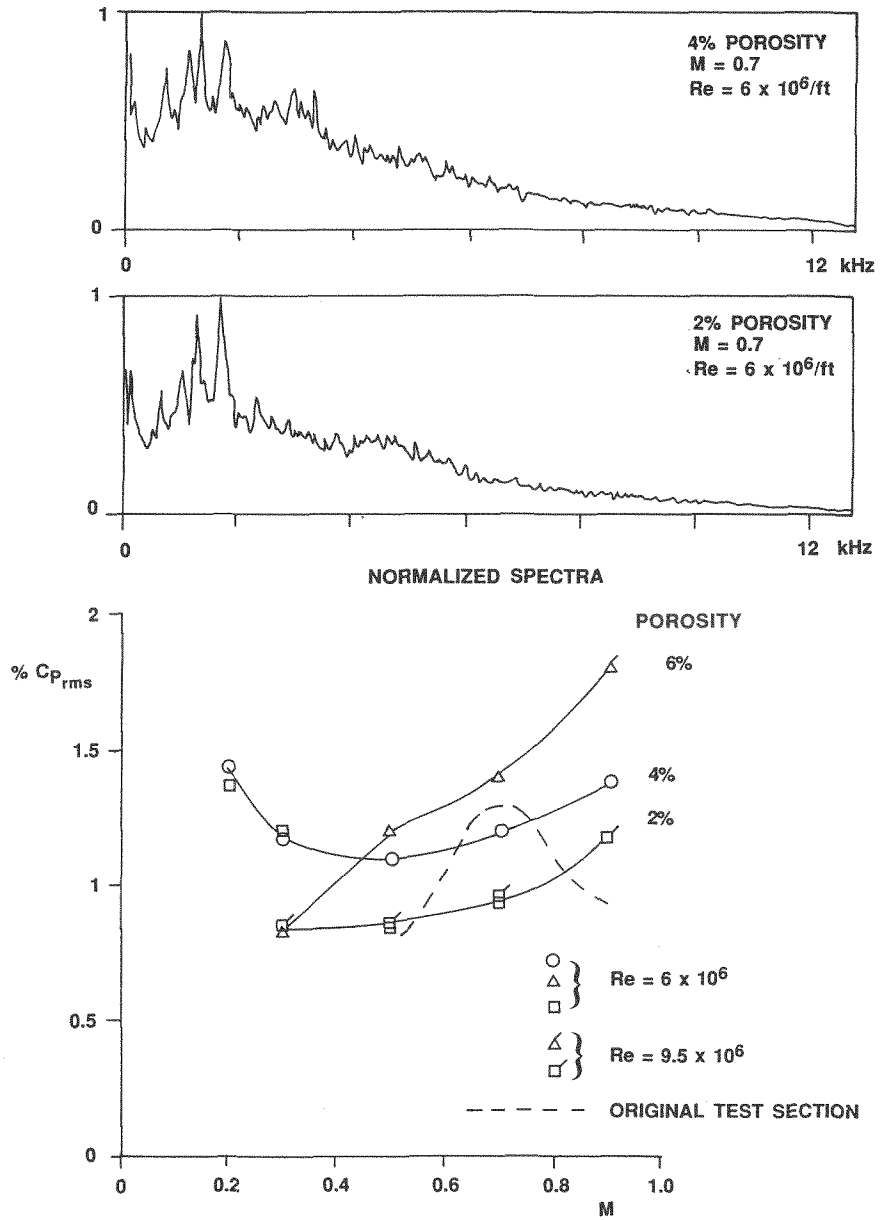

FIG. 12: CENTRELINE STATIC PRESSURE FLUCTUATIONS AND SAMPLE POWER SPECTRA, 3D TEST SECTION

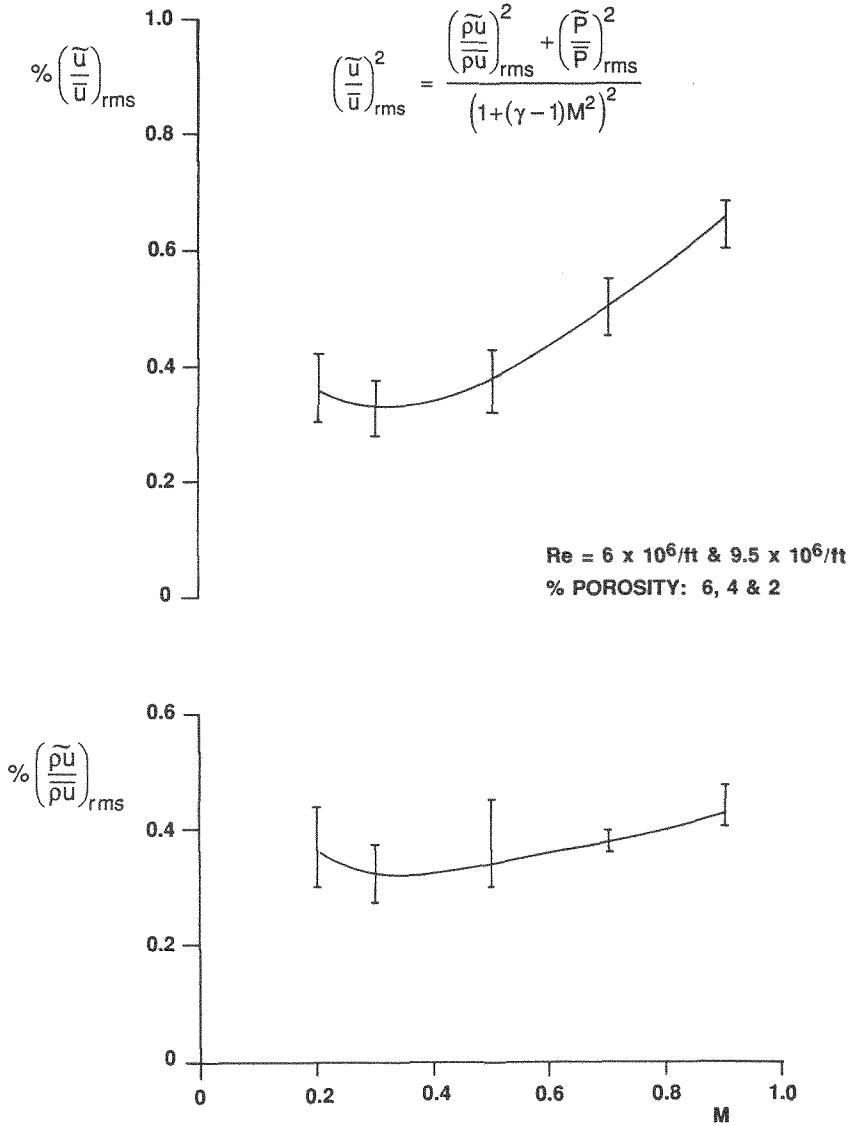

FIG. 13: CENTRELINE MASS FLUX AND VELOCITY FLUCTUATIONS, 3D TEST SECTION

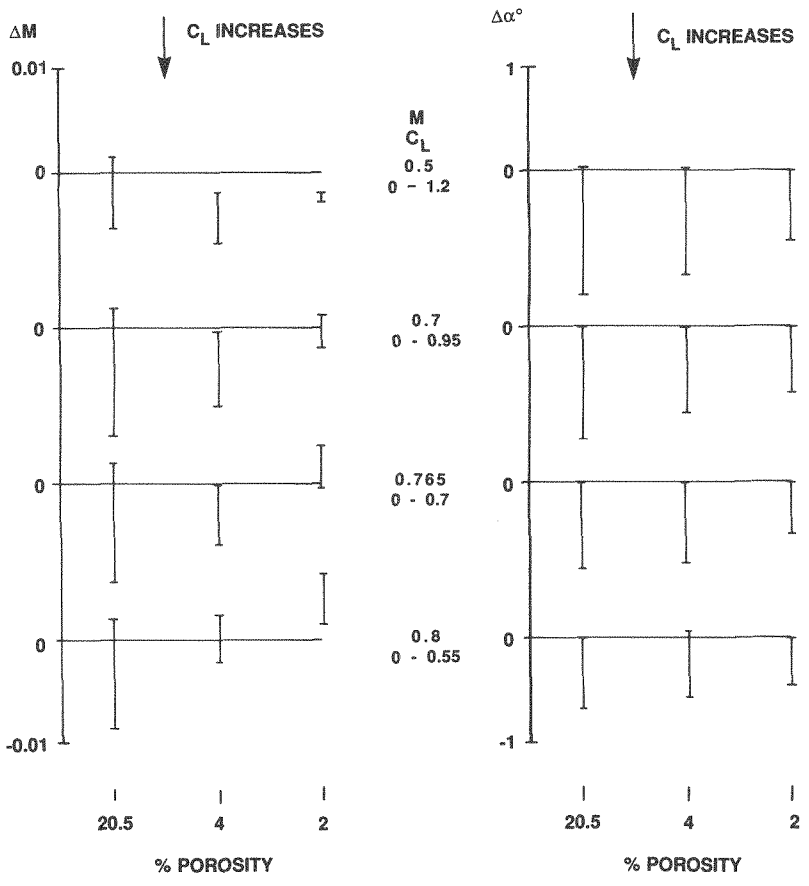

FIG. 14: WALL INDUCED MACH NUMBER AND ANGLE OF ATTACK CORRECTIONS FOR 229mm CHORD AIRFOIL $Re_c = 15 \times 10^6$

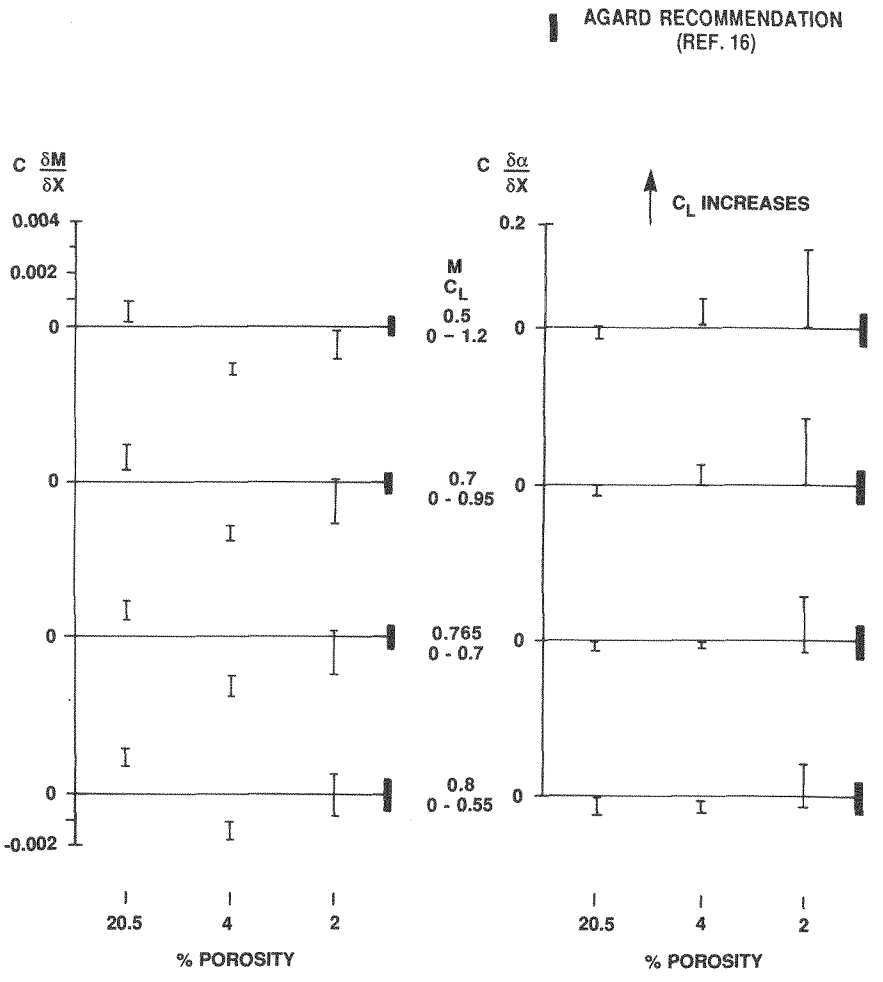

FIG. 15: WALL INDUCED MACH NUMBER AND ANGLE OF ATTACK GRADIENTS FOR 229mm CHORD AIRFOIL $Re_c = 15 \times 10^6$

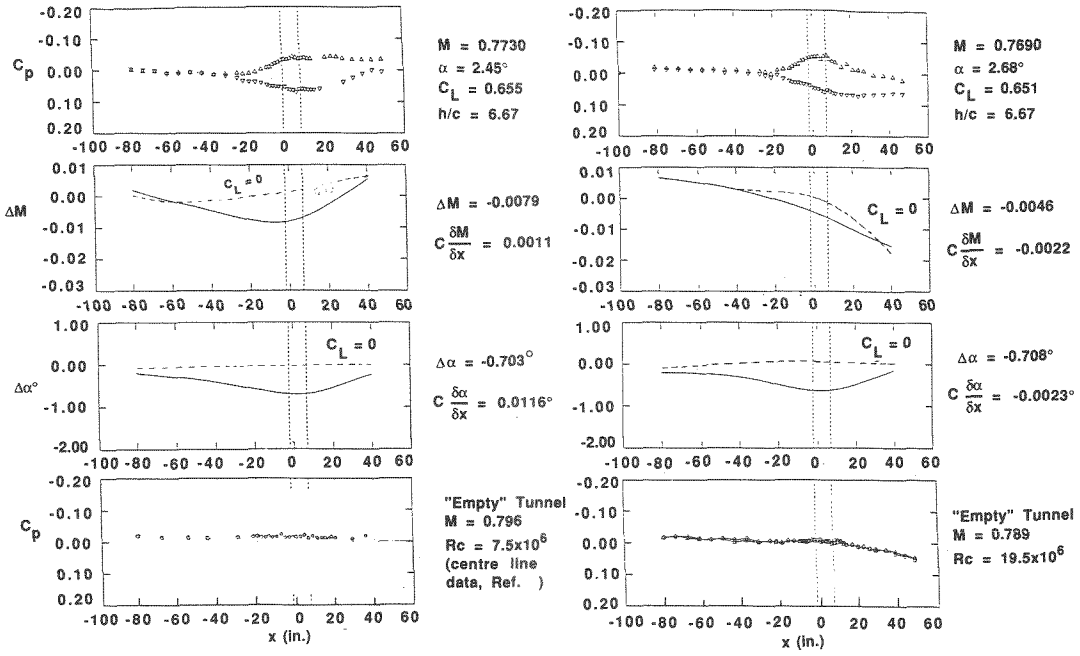

a) 20.5% POROSITY, NORMAL HOLES

b) 4% POROSITY, SLANTED HOLES

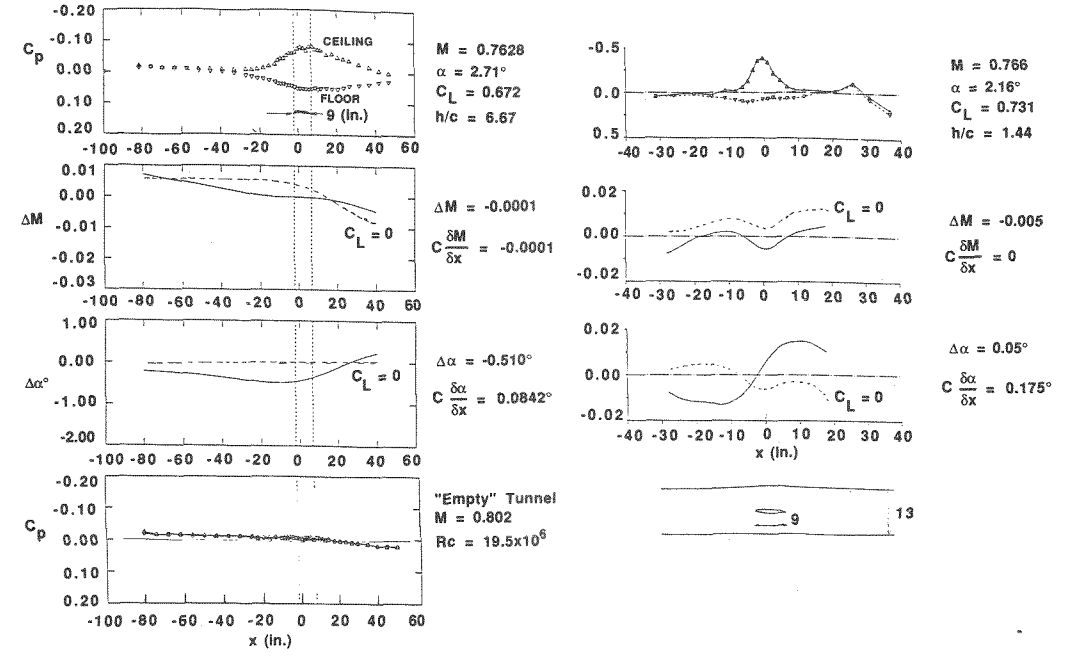

c) 2% POROSITY, SLANTED HOLES

d) ADAPTIVE WALL

FIG. 16: 2D WALL INTERFERENCE RESULTS, $Re_c = 15 \times 10^6$

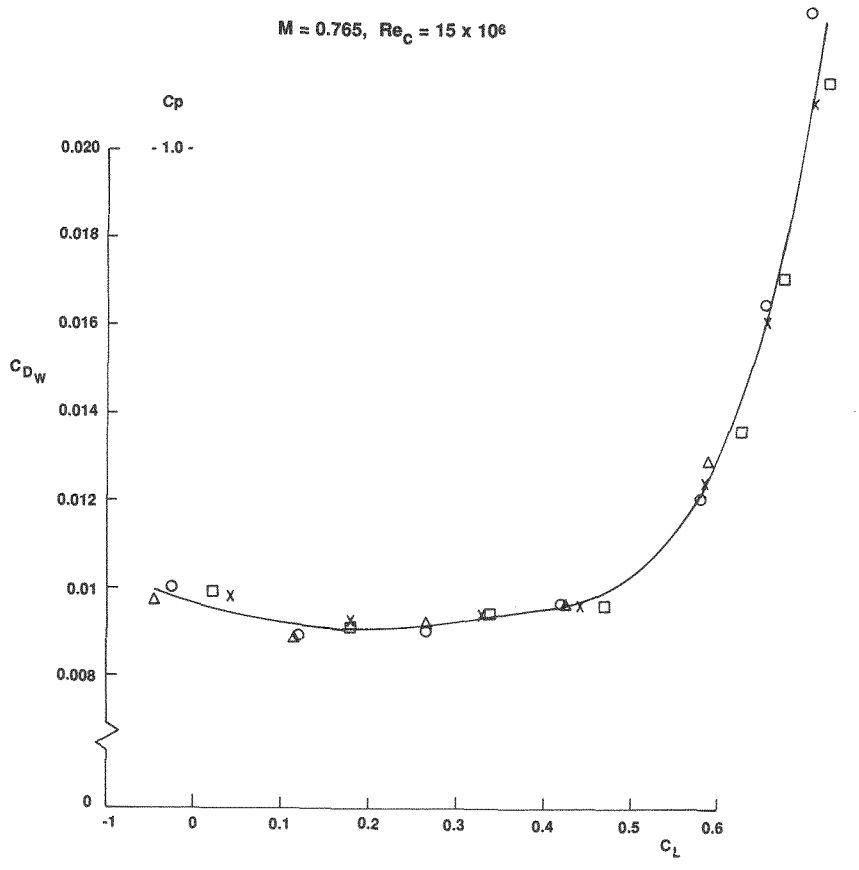

FIG. 17: 2D DRAG POLAR FROM 229mm CHORD AIRFOIL

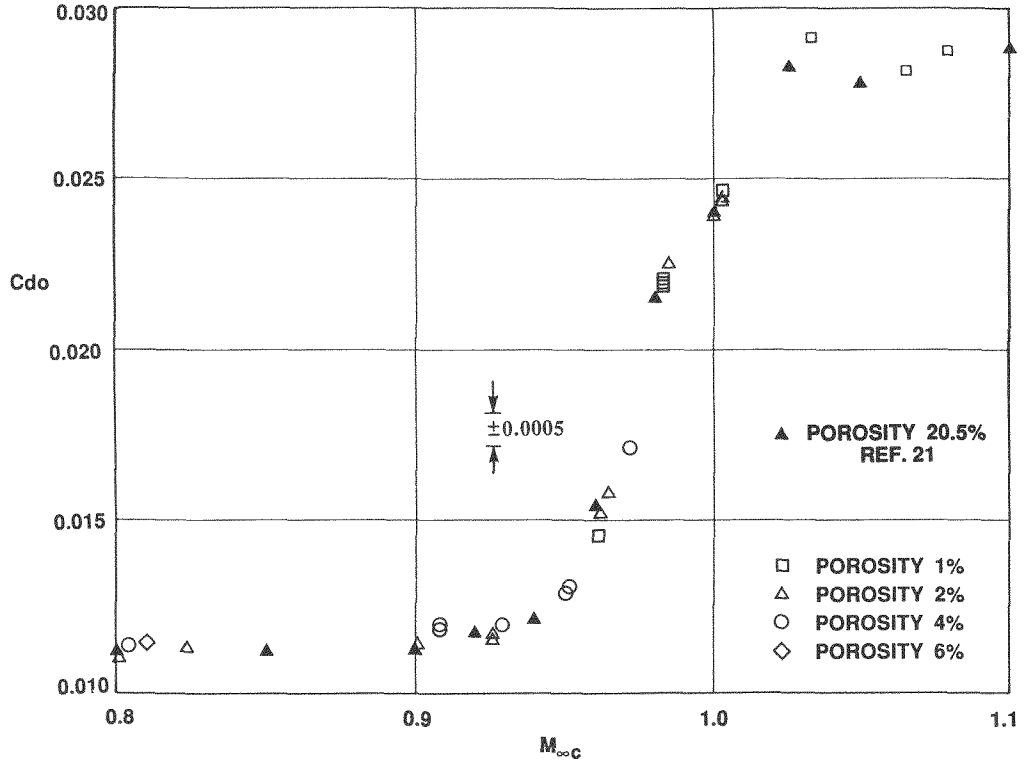

FIG. 18: ZERO LIFT DRAG COEFFICIENT RESULTS
FOR 0.1% BLOCKAGE MODEL WBSC

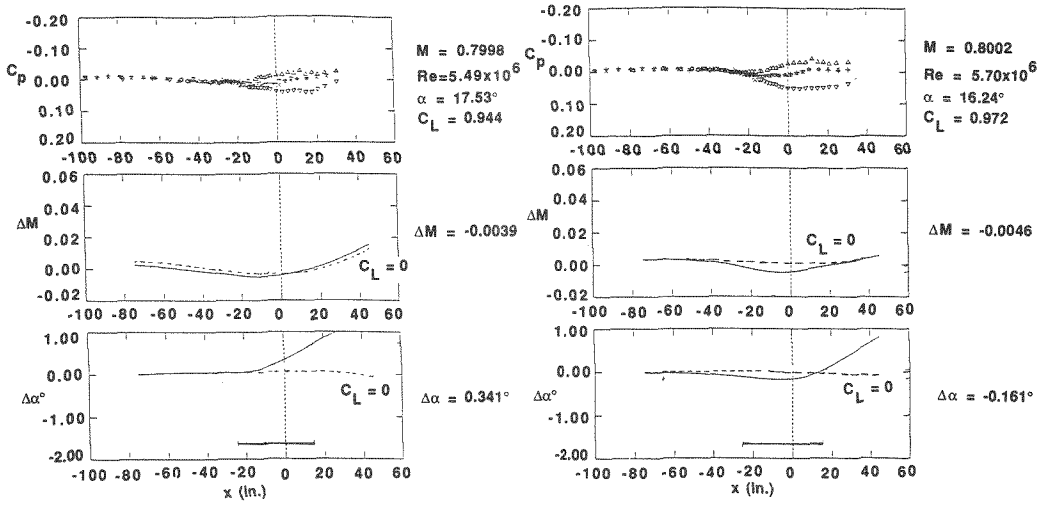

a) 4% POROSITY

b) 2% POROSITY

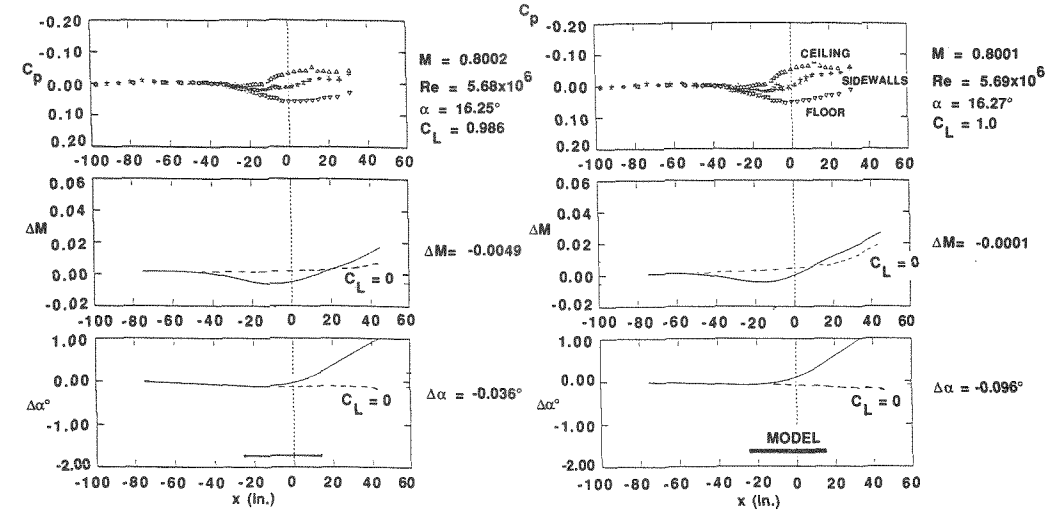

c) 1.5% POROSITY

d) 1% POROSITY

FIG. 19: 3D WALL INTERFERENCE RESULTS, M = 0.8

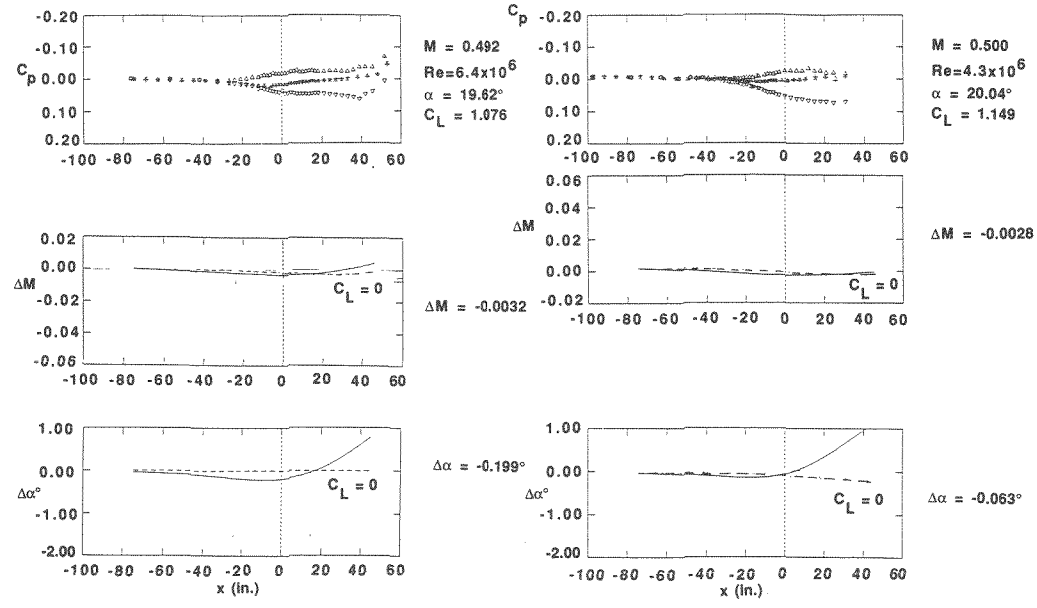

a) 20.5% POROSITY

b) 2% POROSITY

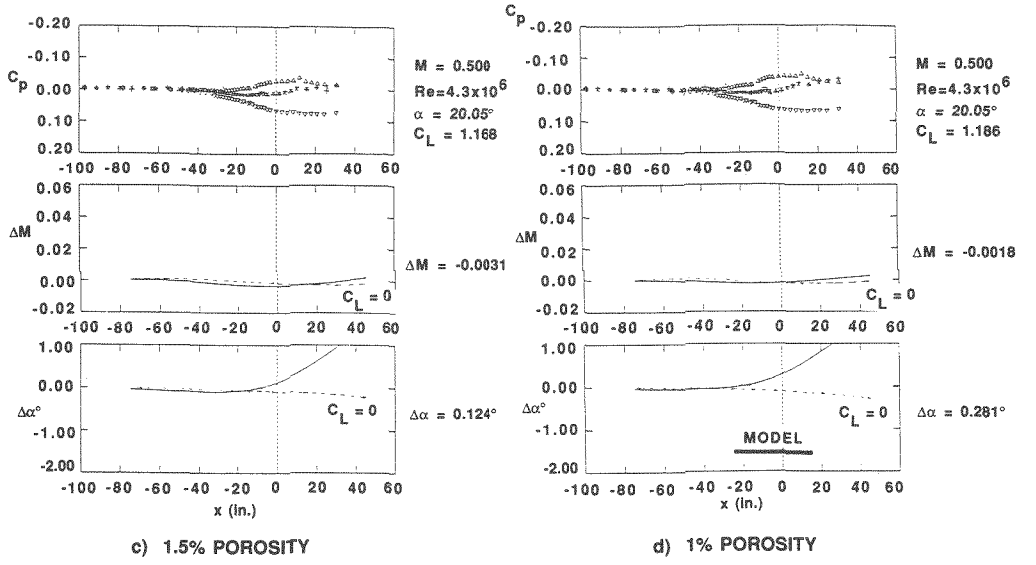

c) 1.5% POROSITY

d) 1% POROSITY

FIG. 20: 3D WALL INTERFERENCE RESULTS, M = 0.5